JOURNAL OF THERMOPHYSICS AND HEAT TRANSFER
Vol. 25, No. 1, January–March 2011

Technical Notes

Nucleate Boiling Heat Transfer on Sintered Copper Porous Structure Module Cone Surfaces

Calvin H. Li*
Villanova University, Villanova, Pennsylvania 19085

DOI: 10.2514/1.49106

Introduction

IN THE past decades, nucleate pool boiling on a flat surface has been extensively studied. Three mechanisms have been identified for the contribution to the enhanced heat transfer efficiency [1,2] of nucleate pool boiling: the transient conduction and replacement of the superheated liquid layer in contact with the heating surface, the evaporation of a liquid microlayer at the base of bubbles, and the circulation of liquid in vicinity of a growing and/or departing bubble. Those mechanisms are closely related to the bubble generation and bubble dynamics. The hydrophilic and hydrophobic surfaces have been used to improve the wettability and bubble growth to enhance the transient conduction and replacement of superheated liquid layer, and hence the evaporation of the liquid microlayer at the base of the bubbles [3,4], and increased active nucleation sites promise a significant heat transfer enhancement on modified porous structure surfaces. Porous structures have been employed in many nucleate-pool-boiling heat transfer studies to increase the active nucleation site number, and many exciting heat transfer enhancements have resulted, such as the sintered copper-mesh and copper-particle porous surfaces [5–10]. Liter and Kaviany [5] have explained the effect of liquid/vapor separation to enhance the critical heat flux of nucleate pool boiling through the modulated porous structure of *n*-pentane. However, the relationship between the heat transfer enhancement and the porous surface characteristics has not been well understood yet.

The heat transfer coefficient of a boiling cycle is first decided by the natural convection regime, where the heating surface area plays a critical role in deciding the magnitude of the heat transfer coefficient. But this critical role of heating surface area gives over to the nucleation site density once the nucleate pool boiling starts, because the boiling heat transfer coefficient is several orders of magnitude larger than the thermal conductivity of copper in the cones, as the effectiveness of the fin is given by $\varepsilon_f = \sqrt{kP/hA}$ [11], where k is the thermal conductivity of copper, P is the perimeter, h is the boiling heat transfer coefficient, and A is the surface area of the cross section. When a large amount of heat conducts through the porous structure, temperature across porous structure slows down its increase, due to the start of nucleate boiling on the nucleation sites. More vapor bubbles will be generated in a porous structure than on a plain surface. The latent heat of liquid/vapor phase change consumes the heat with a small temperature increase. Moreover, with the increase of temperature across the porous structure, more cavities inside the porous structure will be activated, to generate more vapor bubbles, which further increases the heat transfer coefficient of the nucleation pool boiling until no more cavities could be activated. Different from the uniform-thickness porous layers, a cone-modulated porous structure has both cracks and pores. The large cracks provide optimal cavity size for nucleate boiling to occur at a very low superheat temperature and provide vapor ventilation paths at high heat flux. The small pores enhance nucleate pool boiling by adding more active nucleation sites and supply liquid to the large nucleation sites through the capillary pumping effect, which allows occurrence of nucleate boiling in the larger-scale pores through the small inactive pores. In the cone-modulated porous structure, the ascending vapor flow/jet creates a dynamic evaporation surface on the sides of the porous cones to further enhance evaporation efficiency.

In this research, a designed copper-particle sintered porous structure with modulated cones on the top of a thin layer of a plain porous surface has been manufactured, and the nucleate-pool-boiling heat transfer on this structure has been studied. The characteristics of bubble generation, nucleation site density, and heat transfer coefficient under different heating conditions have been analyzed. The results have been compared with that of nucleate pool boiling on a solid flat plate.

Experimental Apparatus and Method

The experimental apparatus used for this study is shown in Fig. 1, which consists of a $200 \times 62.7 \times 67.7$ mm rectangular glass vessel with a copper-plate heating surface at the bottom. Nine T-type thermocouples were inserted into the underside of the copper plate to monitor the temperature of the heating surface and to obtain the heat flux through Fourier's law. Heat flux was supplied by a heating assembly consisting of a 41.5 Ω ceramic-band resistance heater mounted at the bottom of the copper plate, and it was conducted through the copper plate to the heating surface of the glass vessel. The dc power-supply device was an Agilent 6031A. The applied heat flux ranged from 18.9 to 76.3 $\mathrm{kW/m^2}$ during the test. The uncertainty of the temperature measurement was less than 1°C, and the uncertainty of the heat flux was less than 5%. A Redlake MotionScope M3 [charge-coupled-device (CCD) camera] imaging system was employed in the experiment, which had a 520 fps rating of full resolution at 1280×1024 and a maximum of 33,000 fps at a partial resolution of 1280×16. A micro Nikkor lens was used with the CCD camera to take the close-up video of the nucleate-pool-boiling bubble dynamics processes at the view shown in Fig. 1. Although the photographic images were taken through a flat glass wall of the vessel and the filmed phenomena occurred in the region adjacent to the glass wall, they closely represent the bubble dynamics in the inner regions of the bead-packed porous structures in the experiment as well. This is due to the similar geometric structure of the perimeter region and the inner region inside the porous structures, and it was confirmed by visual observation of the nucleate-pool-boiling bubble dynamics experiments. The superheat of the heating surface was measured using nine thermocouples connected to an Agilent 34970A data logger. The data of heat flux against the superheat on the heating surface were calculated simultaneously. Water was used as the working liquid in all the tests.

The modulated porous structure was fabricated with copper particles of an average size of 25 μm on a plain copper surface (as shown in Fig. 2). The modulated porous structure surface is shown in Fig. 3. On the top of the porous structure, there are 72 porous cones arranged in an aligned pattern. The diameter of the cone bottom is 3 mm, the longitudinal and transverse pitches between each pair of the cones are 6 mm, and the height of the cone is 3 mm. The bottom thin porous layer of the structure has a thickness of 2 mm (Fig. 3a).

Received 1 February 2010; revision received 31 October 2010; accepted for publication 2 November 2010.

*Assistant Professor, Department of Mechanical Engineering; Calvin.li@villanova.edu. Member AIAA.

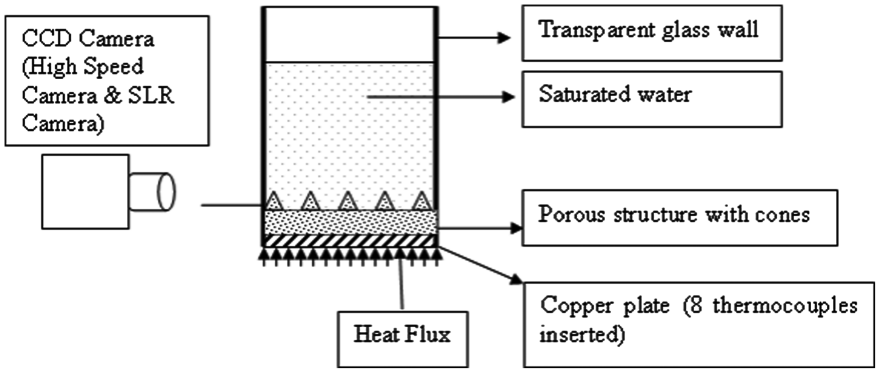

Fig. 1 Sketch of experimental setups (SLR denotes single-lens reflex).

According to the hydrodynamic instability developed by previous studies of Zuber [12], the critical wavelength of the liquid/vapor counterflow is around 2 mm for water, so the distance between each pair of vapor-escaping paths could be ensured by the cone's geometric dimensions that a pair of neighboring vapor-escaping paths will not connect to each other at the critical wavelength and the hydrodynamic instability will be delayed, as evidenced by the study of *n*-pentane nucleate boiling by [3]. The focus of the current study is on the understanding of heat transfer coefficient enhancement by active nucleation site density increase with porous structures.

It clearly shows that there is a 70-μm-wide and 100-μm-deep crack at the feet of porous cones (Fig. 3b and 3d), which is created in the process of sintering. Away from the cracks, the porous structure is well sintered and has an average porosity of 45% (Fig. 3c).

In this test, one band heater and two cartridge heaters were used. The heating-element maximum output power is 440 W. The maximum heat flux is 120 kW/m^2. Because of the high efficiency of the porous covering, the critical heat flux is not reached, even with maximum heat flux.

Result and Discussion

Nucleate Pool Boiling on a Plain Surface

The nucleate pool boiling on a plain surface is presently well understood. In this work, the nucleate-pool-boiling test on a plain surface served as a reference for the staggered-bead porous structure nucleate-pool-boiling investigation. When a small heat flux (18.9 kW/m^2) was applied, it was clear that small vapor bubbles were generated on the plain surface. And with the increase of heat flux, the bubble generation frequency rapidly increased, as shown in Fig. 4a. This bubble dynamics process is unlike the previous report on the subcooled water jet and bubble dynamics process [13], in which the high-temperature water jet existed on the top of large bubbles. When the heat flux was increased to 47 kW/m^2, the vapor generated on the plain surface formed several major vapor slugs and columns, shown in Fig. 4b. At this stage, single bubbles were still detectable by the naked eye. The vapor columns and slugs fit well into the description of the Rayleigh–Taylor hydrodynamic stability theory [14]. There was no obvious collapse between vapor columns, due to the fact that the characteristic size of the columns was still less than the critical hydrodynamic wavelength. When the heat flux was increased to 76.3 kW/m^2, the entire image of the vapor columns could only be recorded with the high-speed camera. A picture of this staged phase-change process is shown in Fig. 4c. The superheat of the nucleate pool boiling on a plain surface changed from 8.22°C at 18.9 kW/m^2 to 22.25°C at 76.3 kW/m^2, as shown in Fig. 5.

The experimental data closely matched the theoretical prediction of pool boiling Rohsenow correlation for saturated water at 1 atm [11], Eq. (1):

$$\Delta T = \frac{h_{f,g}}{c_{p,l}} Pr_l^s C_{sf} \left[\frac{q''_w}{\mu_l h_{f,g}} \left(\frac{\sigma}{g(\rho_l - \rho_v)} \right)^{1/2} \right]^r \tag{1}$$

where ΔT is the superheat on the heating surface, $h_{f,g}$ is the latent heat of water, $c_{p,l}$ is the specific heat of liquid water, Pr is the Prandtl number of liquid water, q''_w is the heat flux on the heating surface, μ_l is the viscosity of liquid water, σ is the surface tension of liquid water, g is gravity, ρ_l is the density of liquid water, ρ_v is the density of water vapor, and C_{sf}, r, and s are constants with values of 0.053, 1, and

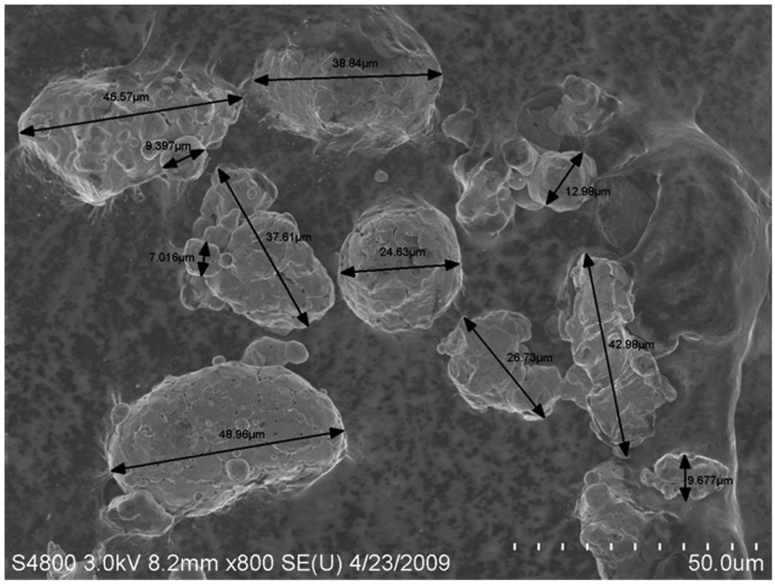

Fig. 2 Scanning electron microscope image of copper particles.

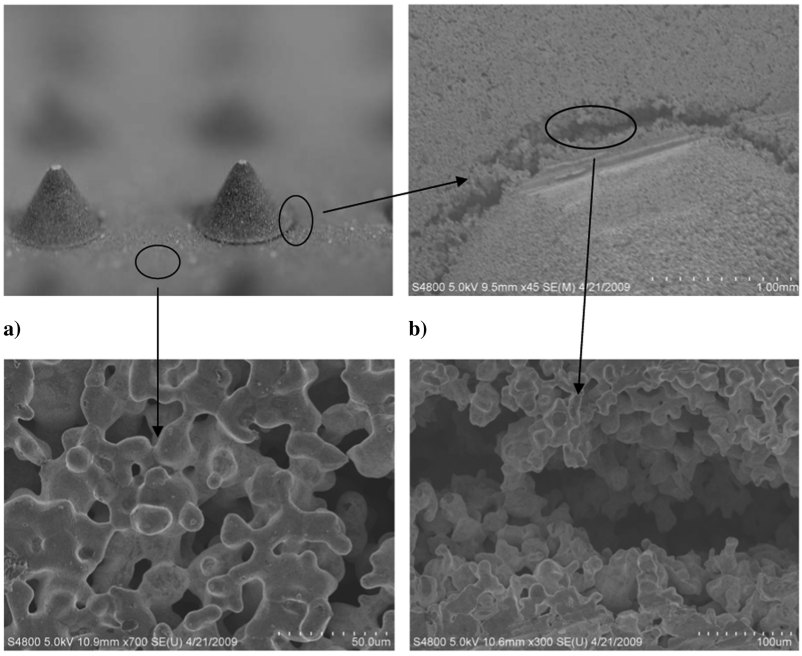

Fig. 3 Porous morphology and cracks in different scales of the cone-modulated structure.

0.66, respectively. The prediction of Eq. (1) is presented as the dashed line in Fig. 4.

Nucleate Pool Boiling on the Modulated Porous Structure

Because of the great heat transfer capacity of copper particles, the sintered copper-particle porous structure greatly enhanced the heat transfer performance, compared with that of a plain copper surface, even in the natural convection regime. After the two-phase heat transfer started, the superheat of the nucleate pool boiling on the modulated porous surface changed from 3.45°C at 31.9 kW/m^2 to 7.6°C at 116.3 kW/m^2. Compared with the superheat under the same order of heat flux on a plain surface, the porous structure surface significantly reduced the superheat. The heat flux increased from 31.9 W/m^2 to 116.3 kW/m^2, almost four times, while the superheat only increased around two times, from 3.45 to 7.6°C.

The visualization pictures illustrated that when the heat flux was low (25.8 kW/m^2), bubbles grew at the foot of the cones from the cracks. Active nucleate sites located at the foot of the cones generated many tiny bubbles with large inertial force and a few relatively large static bubbles located away from cracks (Fig. 6). The reason for bubbles generating at the foot of the cones is that the crack size at the foot of the cones is around 100 μm, as shown in Fig. 3d, which is the optimum cavity size for possible bubble nucleation [15]. Those cracks served as active nucleation sites throughout the test process. Meanwhile, a few static bubbles were observed sitting on the porous surface away from the foot of the cones and another few bubbles were generating at the top of the cones. The size of the top-cone bubbles is

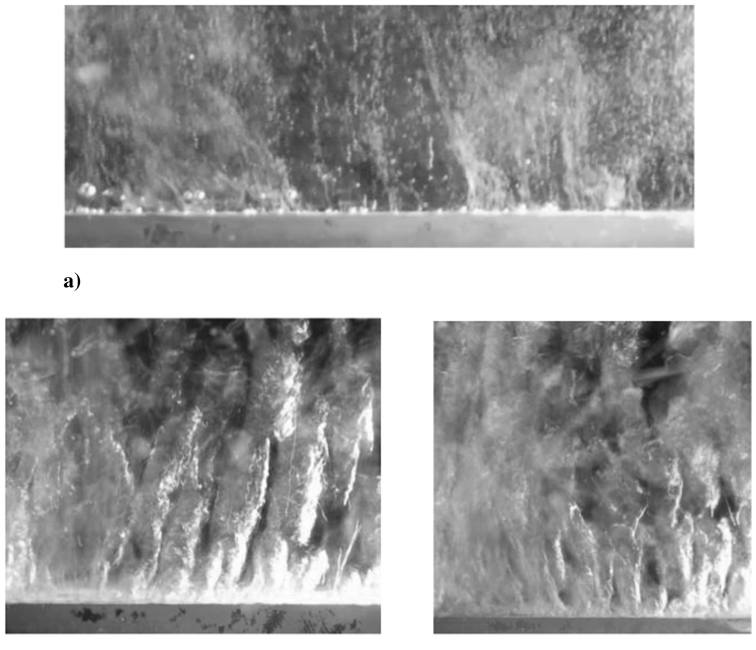

Fig. 4 Bubble dynamics and phase-change nucleate pool boiling on a plain surface.

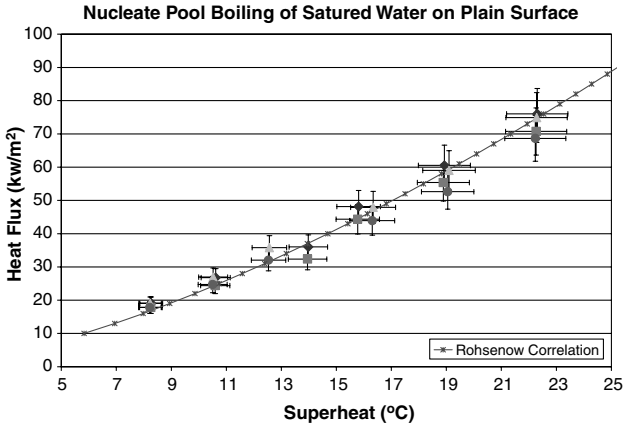

Fig. 5 Heat flux vs superheat on the heating surface of the saturated-water nucleate pool boiling on a plain surface.

smaller than the bubble sitting on the porous surface away from the cracks, but both are stable and do not grow rapidly or depart in a relatively short time period. The reason for these phenomena at low-heat-flux condition is that the thermal energy on the top of the porous surface, especially on the top of the cones, is not sufficient to support bubble growth and departure. The energy was drained away by the tiny bubbles generated at the cracks of the foot of the cones. The high inertial force of these tiny bubbles is due to the rapid two-phase mass change inside the cracks and the V shape of the cracks, where the superheat is very close to the bottom value, and the high heat flux is concentrated at the limited space at the bottom of the cracks. Therefore, numerous tiny bubbles were generated with large inertial energy inside the cracks at the foot of the cones.

With the increase of heat flux, there were more active nucleate sites observed and the tiny bubbles were not visible. The bubble departure size was relative larger and the bubble departure frequency was much slower than that of the tiny bubbles observed at lower heat flux. It is presented in Fig. 7 that bubble coalescence and recoalescence took

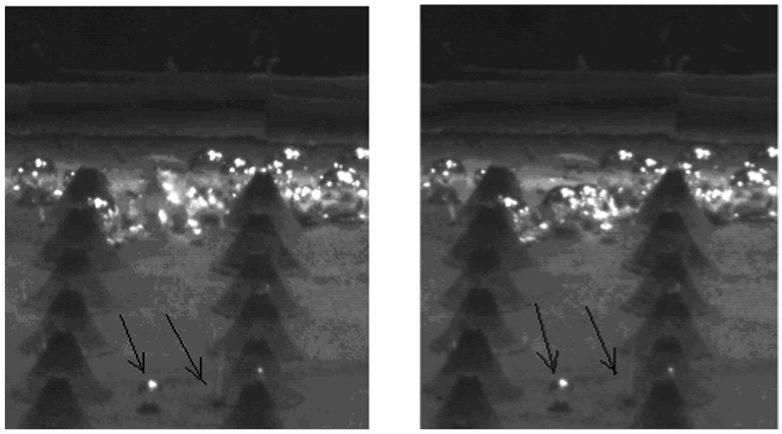

(0 s) **(0.26 s)**

Fig. 6 Nucleate boiling pattern at a heat flux of 25.8 kW/m^2.

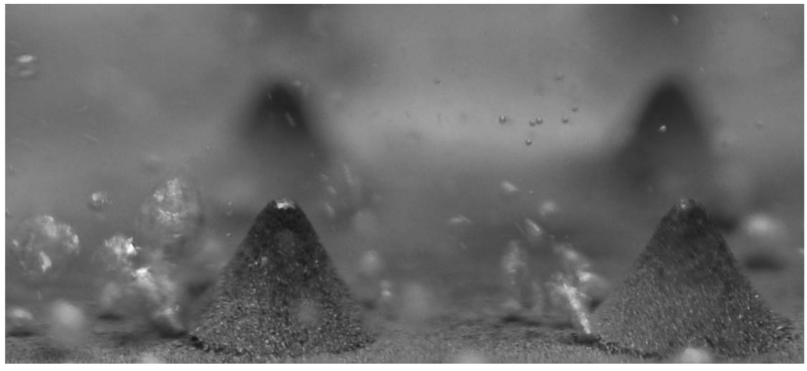

a) 28.8 kw/m^2, 0s

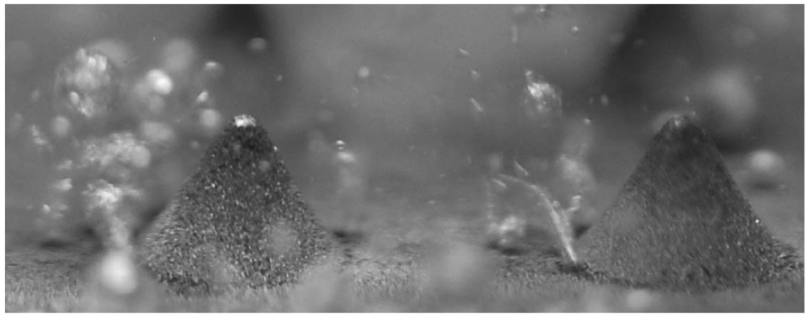

b) 28.8 kw/m^2, 0.33s

Fig. 7 Nucleate boiling pattern at a heat flux of 28.8 kW/m^2.

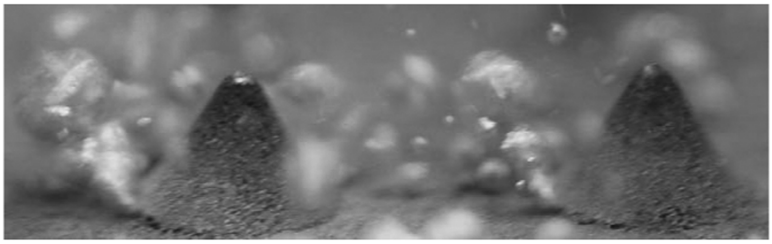

a) 31.7 kw/m2

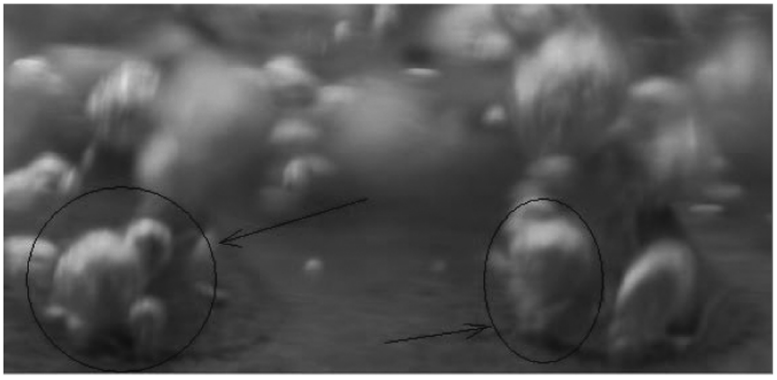

b) 40.6 kw/m2

c) 87.8 kw/m2

Fig. 8 Nucleate boiling pattern at the heat fluxes of 31.7, 40.6, and 87.8 kW/m2.

place to form even larger bubbles. This phenomenon is due to that fact that, with the increase of heat flux, the superheat temperature increased, which led to more two-phase mass transfer and more vapor generated. In turn, the increased heat flux was carried away by more, and slightly larger-size, bubbles generated. However, the bubble generation still happened mostly at the foot of the cones.

By further increasing heat flux, the number of nucleate sites increased, especially at the foot of the cones. So the distances between two nucleate sites at the foot of the cones decreased. When the distance was smaller than a certain value, a bubble column appeared, due to the bubble coalescence among adjacent active nucleate sites at the foot of the cones. It was observed that single-bubble departure frequency and size increased with the increase of heat flux until the bubble column appeared. At a heat flux of 40.6 kW/m^2, it was shown that the big bubble in the right circle had two "feet" contact the heating surface. In the left circle it is clear that there were at least three active nucleate sites sustaining the large bubble that was sitting on the top of them. This mushroom structure started to be more and more dominating in the two-phase heat transfer on the modulated porous structure with the increase of heat flux. At the heat flux of 87.8 kW/m^2, the bubble size further increased, due to the increased bubble coalescence. Larger single bubbles were generated at the same time as bubbles coalesced together to form bubble columns. On the high-heat-flux condition, the bubble size was comparable with, or larger than, the cone size. The heat transfer coefficient continued to increase all the way with the increase of heat flux. Figure 8 demonstrates the bubble dynamics changes in the process of heat flux increase from 31.7 to 87.8 kW/m^2.

It is demonstrated in Fig. 9 that the nucleate pool boiling on a modulated porous structure surface can be divided into the following mechanisms. Inside the porous structure, the capillarity in the pore space will ensure the mass transfer at the bottom of cracks at the foot of the cones under all the heat flux conditions. The porous structure ensures the nucleation sites and extended surface area. The modulated cones on the top of the porous structure regulate the flow pattern of liquid and vapor, which ensures the liquid-water replenishment to the porous structure. As a result, at the same superheat temperature, the heat flux has been dramatically increased; for example, at superheat temperature of 8°C, the plain copper surface has a heat flux of 18.9 kW/m^2, whereas the modulated porous structure surface has a heat flux of 116.3 kW/m^2, almost six times that of the copper plain surface.

As reported by Tolubinskiy [16], the bubble departure diameter D_b is 2.8 mm for water on a copper plain surface, and the bubble departure frequency f_b is 56 s^{-1}. The bubble growth rate is found to be 157 mm/s by multiplying the bubble departure diameter and bubble departure frequency. Those numbers match well with the observations of this experimental study and prediction of the theoretic models [17]:

$$D_b = 1.5 \times 10^{-4} \left[\frac{\sigma}{g(\rho - \rho_g)} \right]^{1/2} (Ja^*)^{5/4} \tag{2}$$

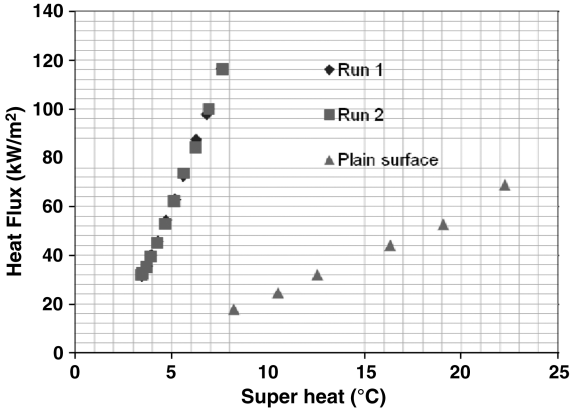

a)

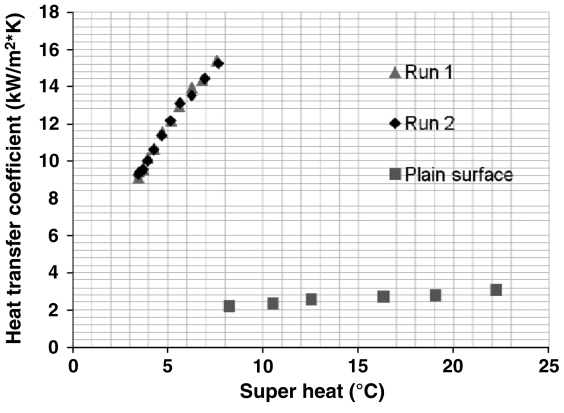

b)

Fig. 9 Boiling curves of the modulated porous structure.

and

$$D_b f_b = 0.6\left[\frac{\sigma g(\rho - \rho_g)}{\rho^2}\right]^{1/4} \tag{3}$$

where σ is surface tension, g is gravity acceleration, ρ is the density of liquid water, ρ_g is density of saturated vapor, and $Ja^* = \rho c_p T_s/(\rho_s h_{fg})$ is the modified Jakob number. The heat flux can be related to the bubble departure through Eq. (4):

$$q = 2\sqrt{\pi k \rho c_p f_b} D_b^2 n \Delta T \tag{4}$$

where k is the thermal conductivity, c_p is the specific heat, n is the number of active nucleation site per unit area, and ΔT is the wall superheat. The number of active nucleation site per area of modulated porous structure is eight times that on a plain copper surface at 8°C superheat, and the number of active nucleation site per area increases with the increase of the wall superheat on a modulated porous structure, whereas it has virtually a constant value on a plain surface.

Conclusions

An experimental study on the two-phase heat transfer on a modulated porous structure has been conducted. The experimental results demonstrated a significant increase in heat transfer performance of this modulated porous structure, compared with that of a copper plain surface. This increase in heat transfer is caused by the liquid capillarity in the small pores, which assisted the liquid-water flow toward the large cracks at the feet of porous cones. More important, the porous structure offers significantly more nucleation sites for the nucleate pool boiling and, in turn, dramatically increases the heat transfer coefficient, compared with nucleate pool boiling on a plain surface.

The cones on the top of the modulated porous structure could help to regulate the liquid-water downward flow and the vapor-bubble upward movement, which helps to avoid the counterflow between the escape of vapor up to the water level and replenishing of liquid down to the bottom of the porous structure once the Rayleigh–Taylor hydrodynamic instability has been reached.

Acknowledgment

The authors would like to acknowledge financial support of this work through Villanova University startup funding.

References

[1] Peterson, G. P., *An Introduction to Heat Pipe: Modeling, Testing and Applications*, Wiley, New York, 1994.

[2] Mikic, B. B., and Rohsenow, W. M., "A New Correlation of Pool-Boiling Data Including the Effect of Heating Surface Characteristics," *Journal of Heat Transfer*, Vol. 91, May 1969, pp. 245–250.

[3] de Genes, P. G., "Wetting: Statics and Dynamics," *Reviews of Modern Physics*, Vol. 57, No. 3, 1985, pp. 827–863. doi:10.1103/RevModPhys.57.827

[4] Tadmore, R., "Line Energy and the Relation Between Advancing, Receding, and Young Contact Angles," *Langmuir*, Vol. 20, No. 18, 2004, p. 7659. doi:10.1021/la049410h

[5] Liter S. G, and Kaviany, M., "Pool-Boiling CHF Enhancement by Modulated Porous Layer Coating: Theory and Experiment," *International Journal of Heat and Mass Transfer*, Vol. 44, 2001, pp. 4287–4311. doi:10.1016/S0017-9310(01)00084-9

[6] Hwang, G. S., and Kaviany, M., "Critical Heat Flux in Thin, Uniform Particle Coatings," *International Journal of Heat and Mass Transfer*, Vol. 49, 2006, pp. 844–849. doi:10.1016/j.ijheatmasstransfer.2005.09.020

[7] O'Connor, J. P., and You, S. M., "A Painting Technique to Enhance Pool Boiling Heat Transfer in FC-72," *Journal of Heat Transfer*, Vol. 117, 1995, pp. 387–393. doi:10.1115/1.2822534

[8] Li, C., Peterson, G. P., and Wang, Y. X., "Evaporation/Boiling in Thin Capillary Wicks, I—Wick Thickness Effects," *Journal of Heat Transfer*, Vol. 128, 2006, pp. 1312–1319. doi:10.1115/1.2349507

[9] Li, C., and Peterson, G. P., "Evaporation/Boiling in Thin Capillary Wicks, II—Effects of Volumetric Porosity and Mesh Size," *Journal of Heat Transfer*, Vol. 128, 2006, pp. 1320–1328. doi:10.1115/1.2349508

[10] Li, C. H., Ting, Li, Paul Hodgins, and Peterson, G. P., "Characteristics of Pool Boiling Bubble Dynamics in Bead Packed Porous," *Journal of Heat Transfer* (to be published).

[11] Incropera, F. P., DeWitt, D. P., Bergman, T. L., and Lavine, A. S., *Fundamentals of Heat and Mass Transfer*, Wiley, New York, 2007.

[12] Zuber, N., "Hydrodynamic Aspects of Boiling Heat Transfer," Ph.D. Thesis, Univ. California, Los Angeles , Los Angeles, 1959.

[13] Wang, H., Peng, X. F., Christopher, D. M., Lin, W. K. and Pan, C., "Investigation of Bubble top Jet Flow During Subcooled Boiling on Wires," *International Journal of Heat and Fluid Flow*, Vol. 26, 2005, pp. 485–494. doi:10.1016/j.ijheatfluidflow.2004.09.005

[14] Drazin, *Introduction to Hydrodynamic Stability*, Cambridge Univ. Press, New York, 2002.

[15] Rohsenow, W. M., "A Method of Correlating Heat Transfer Data for Surface Boiling of Liquids," *Transactions of the ASME*, Vol. 84, 1962, pp. 969–976.

[16] Tolubinskiy, V. I., *Heat Transfer Under Boiling*, Naukova Dumka, Kiev, Ukraine, 1908.

[17] Mikic, B. B., and Rohsenow, W. M., "A New Correlation of Pool-Boiling Data Including the Effect of Heating Surface Characteristics," *Journal of Heat Transfer*, Vol. 91, 1969, pp. 245–250.